A Numerical Study of Mass Transfer in Free Falling Wavy Films

Numerical simulations of mass transfer into falling liquid films, both through the wavy interface and from the wall, have been performed for experimentally measured large waves within which the flow fields have been computed. Experiments have shown that the occurrence of waves on free falling films causes dramatic increases in mass transfer into the film, even under laminar flow conditions. Wave effects have been modeled in several ways, none of which predicts the observed rate of enhancement. The present numerical procedure includes solving the convective-diffusion equation for wavy films by extending a technique developed for hydrodynamic simulation. The presence of waves is shown to cause significant velocities normal to each interface. In conjunction with recirculation within the large waves, these flow patterns produce transfer rates for large waves that are several times larger than predicted for quasiparallel velocity fields. Experimental wave structure data were used to define the dimensions and frequency of an average large wave and surrounding substrate. Computed transfer rates at both the gas-liquid interface and the wall for a film composed of a periodic sequence of average waves agree well with published data. These simulations confirm the inadequacy of parabolic, or Kapitza-type velocity profiles in formulating transport models.

Frederic K. Wasden
A. E. Dukler
Department of Chemical Engineering
University of Houston
Houston, TX 77204

Introduction

The ability of liquid films to transfer large amounts of heat or mass with low hydraulic resistance has led to their use in a wide variety of industrial processes. For unit operations in which the liquid phase is distributed as a film, the throughput of the unit is often determined by the liquid-phase transport resistance; trickle-bed and falling-film reactors, wetted-wall absorbers, and vertical evaporators are examples. Upon contacting a solid surface, liquid films quickly evolve to a complex array of waves whose amplitudes vary from much less to much greater than the mean thickness. This gravity-driven behavior is observed for all flow rates of industrial importance, even in the absence of interfacial stresses due to adjacent gas flow. Figure 1 shows a sample time tracing of the interface of a fully developed laminar film falling freely down a vertical tube without gas flow. The presence of large waves flowing over a thin substrate which itself is covered by small waves is clearly displayed.

Mass transfer in liquids is characterized by extremely long time scales for molecular diffusion. The ratio of thermal to molecular diffusivities in liquids is generally greater than 100, suggesting that mass transfer rates reflect fluctuations in flow field to a greater extent than do heat transfer rates. This speculation has been confirmed by reviews of experimental studies (Seban and Faghri, 1978; Henstock and Hanratty, 1979). This disparity is exploited in the present work to provide a comprehensive examination of a combination of numerical procedures.

A simplified view of a liquid film suggests that transport is limited by diffusion in the direction normal to the transfer surface. The velocity of a contaminant traveling normal to the interface as the result of diffusion is of the order of the ratio of the diffusivity to the film thickness. The comparable velocity in the streamwise direction due to advection is of the order of the average film velocity. The ratio of the advective to the diffusive

F. K. Wasden is presently with Shell Development Company, Westhollow Research Center, Houston, TX.

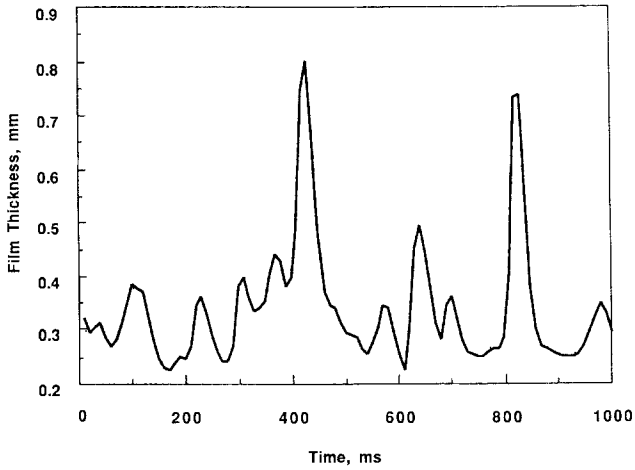

Figure 1. Film thickness time trace, $Re = 880$.

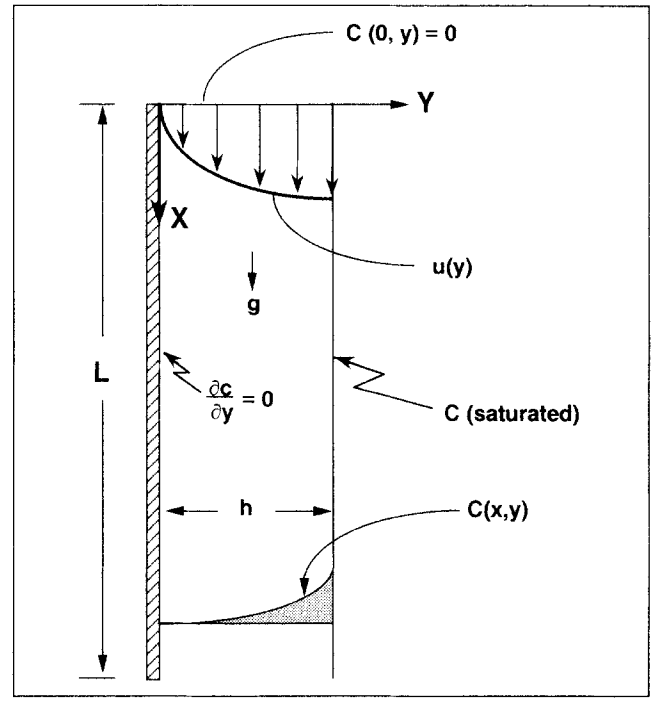

Figure 2. Absorption through the surface of a flat film.

velocity, the Peclet number, is of order 10^4–10^6 for industrially important thin film flows. Experiments have shown that the presence of waves on films causes dramatic increases in heat or mass transfer, even for laminar flows. While a wide range of wave amplitudes exists, it is speculated that the large waves, ranging from two to five times the substrate thickness in amplitude, control the transport rates (Dukler, 1977).

Predicting the enhancement of transport rates due to the wavy interface has provoked many studies of film hydrodynamics. Since first being addressed by Kapitza and Kapitza (1949), studies of the linearized hydrodynamics within wavy films have yet to predict the wide variety of wave shapes, sizes, and speeds observed experimentally. Numerical studies of the problem are limited. Bach and Villadsen (1984) succeeded in predicting velocity profiles in traveling waves using a finite-element technique, but their results were limited to Reynolds numbers less than 100. The film Reynolds number is defined as $Re = 4Q/\nu$, where Q is the mass flow rate per unit perimeter and ν is the kinematic fluid viscosity. Recent numerical studies of hydrodynamics in isolated and interacting large waves at a Reynolds number of 880 (Wasden and Dukler, 1989a, b) have provided information on the flow fields existing in these waves. The hydrodynamic studies predict regions of large streamwise acceleration in the waves as well as recirculating zones. Nakaya (1989) has also found these flow patterns in large waves at low flow rates.

This study focuses on numerical prediction of mass transfer to laminar free falling films for both gas absorption at the free surface and dissolution at the wall in the presence of complicated velocity fields. The former situation has been studied extensively, both experimentally and theoretically, and is reviewed by Henstock and Hanratty (1979). Information on the wall transfer is much more limited.

Existing Models and Experimental Studies

Mass transport in flat films

Early attempts at describing transport in films were limited to situations where the film was assumed to be flat. Transfer from the adjacent gas phase into the film through the free interface is illustrated in Figure 2. The transport is governed by the convective-diffusion equation, which can be written in two dimensions as

$$\frac{\partial c}{\partial t} + u\frac{\partial c}{\partial x} + v\frac{\partial c}{\partial y} = D\left(\frac{\partial^2 c}{\partial x^2} + \frac{\partial^2 c}{\partial y^2}\right) \tag{1}$$

where $c(x, y, t)$ is the concentration of the species and $u(x, y, t)$ and $v(x, y, t)$ are the velocity components in the streamwise (x) and normal (y) directions. For steady flat film flow, the parabolic velocity profile is used for the axial velocity and the convective-diffusion equation reduces to

$$u(y)\frac{\partial c}{\partial x} = \frac{gh^2}{\nu}\left(\frac{y}{h} - \frac{y^2}{2h^2}\right)\frac{\partial c}{\partial x} = D\left(\frac{\partial^2 c}{\partial y^2}\right) \tag{2}$$

where streamwise diffusion is negligible at the high Peclet numbers experienced in practice. For absorption, the boundary and initial conditions assume an initially pure solution with a saturated interfacial condition and no flux at the wall:

$$c(x, y) = 0 \quad \text{at} \quad x = 0 \text{ for all } y \tag{3a}$$

$$c(x, h) = c_{\text{saturated}} = c_s \quad \text{at} \quad y = h \text{ for all } x \tag{3b}$$

$$\frac{\partial c}{\partial y} = 0 \quad \text{at} \quad y = 0 \text{ for all } x \tag{3c}$$

The first analytical solution of Eqs. 2 and 3 was presented by Pigford (1941), who assumed that the gas–liquid contact time was short enough that variations in concentration occur only in a boundary layer near the free interface. Replacing the condition of Eq. 3c with $c(x, 0) = 0$ enabled him to find a closed-form solution for the local mass flux at any position x, and for the mass flux averaged over a column length of L. The latter solution

is given below and is referred to as the short contact time theory (SCTT) mass transfer rate,

$$N_{SCTT} = c_s \sqrt{\frac{2Dgh^2L}{\nu\pi}} \tag{4}$$

Mass transfer from the solid wall into the falling liquid film is seldom encountered in industrial practice, although its analog, the process of heat transfer from the wall is quite common. Figure 3 illustrates the mass transfer situation for a flat film in which a portion of the wall is considered to be active, or capable of supplying mass to the film. Boundary and initial conditions are similar to those for the absorption problem. An initially pure solvent is assumed to be saturated at the liquid–solid interface and no transport is allowed at the free interface:

$$c(x, y) = 0 \quad \text{at} \quad x = 0 \tag{3a}$$

$$c(x, 0) = c_s \quad \text{for} \quad y = 0, \quad 0 < x < L_A \tag{5a}$$

$$\frac{\partial c}{\partial y} = 0 \quad \text{at} \quad y = h \tag{5b}$$

$$\frac{\partial c}{\partial y} = 0 \quad \text{at} \quad y = 0 \quad \text{for} \quad x > L_A \tag{5c}$$

No general analytical solution to the governing equations exists for arbitrary lengths of the active region, L_A. For small diffusivities (large Schmidt numbers) and small contact times, a boundary layer analysis similar to Pigford's was proposed by Acrivos (1960). In the limit of low Peclet numbers (high mass diffusivity), Spence and Brown (1968) solved the transport problem using a Frobenius series to solve the ordinary differential equation generated by the Laplace transform of the original partial differential equation. In principle, this method can be extended to the general case, but the Frobenius series does not possess sufficiently robust convergence characteristics to allow its use.

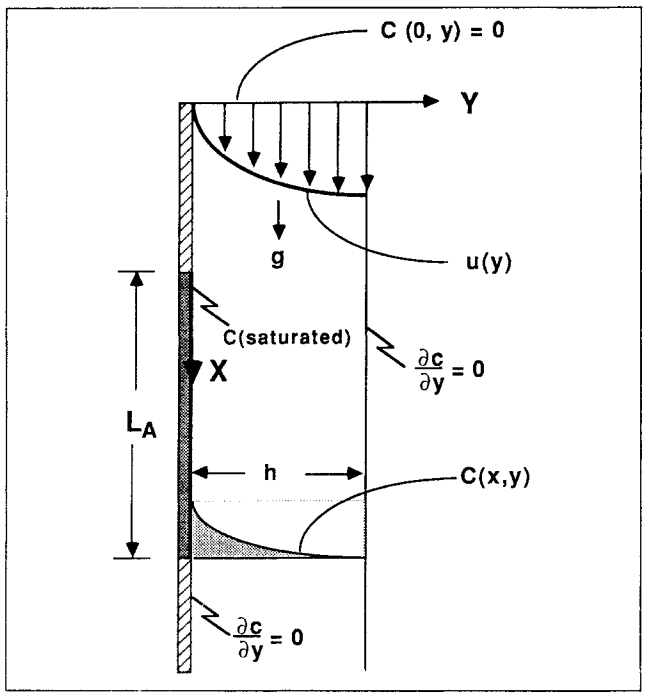

Figure 3. Mass transfer from solid boundary into flat film.

Gas absorption through the wavy interface

Most gas absorption experiments that have been reported provide information on mass flux or mass transfer coefficients averaged over the entire length of film. Simultaneous local measurements of time-varying wavy film thickness and concentrations have not been reported, so little information is available on the local transport process. Emmert and Pigford (1954) reported mass transfer rates in agreement with short contact time predictions, Eq. 4, when a surfactant was added to suppress waves. In the absence of surfactant, mass transfer rates two to three times greater than observed for flat films were measured for Reynolds numbers of 200–1,200 and Schmidt numbers between 400 and 500 in a column 1.1 m long.

Kafesjian et al. (1961) examined the rates at which a species is absorbed and desorbed from a film. No equivalent to the short contact time theory exists for desorption since the concentration is uniform in the incoming fluid. Measured values of desorption from the film suggest an additional 20–30% enhancement over the absorption rate computed from correlations of Emmert and Pigford, implying that waves do more than stretch and contract the velocity profile. By imposing external disturbances and generating standing waves of various amplitudes and frequencies on stationary horizontal films, Goren and Mani (1968) measured mass transfer rates greater than ten times the values expected for smooth films, with increases scaling roughly linearly with wave amplitude.

Data from a variety of investigators published over a three-decade period were correlated to film Reynolds number and Schmidt number by Henstock and Hanratty (1979). The data reflect a variety of columns sizes, with Schmidt numbers ranging from 250 to 1,200 and Reynolds numbers from 100 to 10,000, encompassing laminar and turbulent films. The ratio of the mass transfer coefficient from their correlation to that of the short contact time solution, $k_{L,SCT}$, is:

$$E = \frac{k_L}{k_{L,SCT}} = 0.0111 \sqrt{\frac{(L/h_N)}{Re}} [(0.707 \sqrt{Re})^5 + (0.0310^{0.9}\sqrt{Re})^5]^{0.30} \tag{6}$$

where k_L is the liquid side mass transfer coefficient averaged over the film length L and h_N is the Nusselt or time-averaged film thickness. Equation 4 can be used to show that

$$k_{L,SCT} = \sqrt{\frac{3\,D\,\nu\,Re}{2\pi\,L\,h_N}} \tag{7}$$

The enhancement, E, depends only on film Reynolds number and length, varying from 1.15 for L/h_N of 3,000 and Reynolds number of 100 to 2.9 for L/h_N of 10,000 and Reynolds number of 1,000. An enhancement of nearly fifteen times is predicted for a turbulent film with a Reynolds number of 10,000 and length L/h_N of 10,000. The additional interfacial area due to the waves over that of a flat interface has been shown to be negligible over a wide range of flow rates (Portalski and Clegg, 1971), so the

enhancement in Eq. 6 is not influenced by differences in interfacial area due to the presence of waves.

The modeling of gas absorption in falling films has proceeded along four paths.

1. Levich (1962) extended the short contact time solution to allow the surface velocity to vary with film thickness. Treating the interface as a periodic array of small-amplitude traveling capillary waves, Levich used the model of Kapitza and Kapitza (1949) to predict the surface velocity and concluded that the enhancement, E, would be about 1.15. Ruckenstein and Berbente (1965, 1968) also used the Kapitza hydrodynamic model and approximated the interface as small-amplitude traveling waves described by two Fourier modes. The concentration profile in the film was approximated by a power series in the coordinate normal to the interface and an enhancement of about 30% was predicted. Since the Kapitza wave model describes only capillary waves the results are applicable only for very low Reynolds numbers.

More recently, Barrdahl (1988) solved the convective-diffusion equation for transport into wavy films at very low Reynolds numbers, near the condition of wave initiation. He showed that mass transfer enhancement due to small waves scales with $Pe^{1/2}$. Howard and Lightfoot (1968) arrived at the same conclusion by treating the interface as a periodically stretching surface. Javdani (1974) suggested a model for wave-induced concentration fluctuations similar to simple eddy viscosity models. Using the Kapitza model for the velocity profile he proved only that enhancement scales as $Pe^{1/2}$.

2. The models discussed above are deficient in their neglect of the presence of large roll waves and the substantial velocities normal to the interface that can be expected to accompany them. Attempts to relate the increased mass transfer to large wave properties using surface renewal models are summarized by Davies (1972) and Dukler (1977). Banerjee et al. (1967) proposed a renewal model which assumed that the large waves mixed with the substrate over which they passed, bringing fresh solution to the interface. Closing the problem required a relation between the Reynolds number and large-wave frequency; this was derived from linear stability considerations. Since linear stability analyses characterize only small capillary waves (Benjamin, 1957), this choice of relationships is questionable. The model was modified by Brumfield et al. (1975), incorporating new data on large-wave frequencies (Telles and Dukler, 1970).

3. Wave-induced turbulence was suggested by Suzuki et al. (1983) as a means of explaining the enhanced mass transfer rates. The method proposed a turbulent diffusivity for both large and small waves whose definition was empirically related to the size and velocity of the waves. Poor agreement between predicted and measured transport rates was reported for instances in which this model was applied to flows with many large waves.

4. Films sheared by the surrounding gas have been studied experimentally (McCready and Hanratty, 1985) and analytically (McCready et al., 1986; Back and McCready, 1988). It is suggested that shear stress variations due to gas flow around waves induce normal velocities near the interface which influence mass transfer. Of course, this mechanism is not applicable to the case of free falling films.

The experimental evidence accumulated over the past three decades shows that mass transfer enhancement due to waves on films cannot be explained with models using any variant of the Kapitza capillary wave velocity profile. Models based on large-wave-induced surface renewal suffer for lack of a complete characterization of wave structure, frequency, and amplitude distribution. Analyses based on more robust hydrodynamic models appear to be the logical next step toward reconciling experimental measurements and predicted transfer rates.

Mass transfer from the wall

Few experimental studies of this problem have been reported. Referring to Figure 3, most experiments have been conducted with a contaminant affixed to a tube wall or flat plate over a distance L_A. A film was allowed to flow over the solute, with careful attention to complete wetting of the surface. Mass transfer rates were determined either by weighing the plate before and after the experiments or by measuring the outlet bulk concentration of the fluid.

Stirba and Hurt (1955) attempted to relate the increased transfer rate due to the waves to a universal eddy diffusivity. Experiments in 2 m long tubes coated with organic acids over lengths from 1 to 1.5 m showed apparent diffusivities ranging from three to twenty times the molecular diffusivity, depending on the Reynolds and Schmidt numbers. Reynolds numbers in the study varied from 300 to 3,000, and Schmidt numbers from 600 to 18,000. No general correlation of the results was presented.

Oliver and Atherinos (1968) conducted experiments in an inclined channel at angles of 30° or less with the horizontal, $Re < 200$, and length of about 0.3 m. They found that transfer rates were described adequately by a short contact time, smooth liquid film theory analogous to that of Pigford for gas-liquid transfer. However, the conditions of the experiment were such that large waves were not present. Oliver and Atherinos suggest that the difference between their result and that of Stirba and Hirt is due to the presence of large waves in the latter experiments while theirs only showed capillary wave motion.

Mass transfer from a wall to a liquid is represented by a substantial body of literature because of interest in the use of electrochemical probes to measure wall shear stress (Hanratty and Campbell, 1983). However, these models all assume the existence of a very thin concentration boundary layer near the wall through which the velocity profile can be assumed to be linear. This condition is a very specialized one and not of general applicability. No analytical theories exist that can be used to explore the effect of wave motion on this wall to fluid transfer. Speculation about the effect of large waves on transfer rates is possible through an examination of the velocity profile near the wall, where the streamwise velocity can be approximated using a Taylor expansion,

$$u(x, y, t) \approx u(x, 0, t) + \left(\frac{\partial u}{\partial y}\right)_{(x,0,t)} y + \ldots \tag{8}$$

where $u(x, 0, t)$ is identically zero, and the derivative term represents the wall shear stress. Using the continuity equation, the normal velocity is seen to be approximated by

$$v(x, y, t) \approx \frac{y^2}{2} \frac{\partial}{\partial x}\left(\frac{\tau_w}{\mu}\right) \tag{9}$$

This simple scaling shows that mass transport enhancement is expected near the front and rear or large waves, where wall

shear stress values are rapidly changing (Wasden and Dukler, 1989a, b).

Computational Procedure

The numerical study focused on simulating mass transfer in a series of seven experimentally measured large wave shapes chosen from film thickness traces obtained at a Reynolds number of 880. The wave shapes chosen included both isolated and interacting waves and were representative of all large waves existing on the film. Simulation of mass transfer through either the wavy interface or from the wall combined three numerical algorithms. First, the u and v velocity fields were computed for each wave using a finite-difference numerical algorithm based on the TEACH-T code (Gosman and Ideriah, 1976) and described elsewhere (Wasden and Dukler, 1989a, b). The hydrodynamic simulation was performed under the assumption of passive scalar transport, that is, the presence of the diffusing species did not affect the physical properties of the fluid. Boundary conditions required to specify the concentration distribution in the flat film surrounding the large waves were then computed from a numerical solution of Eqs. 2 and 3 or Eqs. 2 and 5. The final step in the transport simulation was the solution of the convective-diffusion equation using the velocity and spatial shape profiles determined in the hydrodynamic simulations.

Gas absorption through the wavy interface

The gas absorption problem simulated in this study is illustrated in Figure 4. Each large wave is modeled as being surrounded by a flat film in which the concentration field is described by the solution of the flat film problem, Eqs. 2 and 3, for a given position of the wave in the column, L. Mass transfer through the wavy interface is computed as the wave passes a location L below the feed. A locally variable wave velocity, $V_w(z)$, is determined in the course of the hydrodynamic simulation and used to approximate the unsteady terms in Eq. 1,

$$\frac{\partial c}{\partial t} = -V_w(z)\frac{\partial c}{\partial z} \tag{10}$$

The solution is then generated for a steady problem in a coordinate system moving with the wave. The convective-diffusion equation for this planar flow is then written

$$(u - V_w)\frac{\partial c}{\partial z} + v\frac{\partial c}{\partial y} = D\left(\frac{\partial^2 c}{\partial z^2} + \frac{\partial^2 c}{\partial y^2}\right) \tag{11}$$

where the coordinates are shown in Figure 4. At the solid boundary, $y = 0$, a no-flux condition, Eq. 3c, is imposed while the free surface streamline corresponds to a saturated solution, Eq. 3b. The inlet condition, at $z = L$, is determined by a numerical solution of Eqs. 2 and 3 for given Peclet number, substrate thickness, and fluid properties. The outlet condition, at $z = L - \lambda$, corresponds to negligible steamwise concentration gradients, or

$$\left(\frac{\partial c}{\partial z}\right)_{z=L-\lambda} \approx 0 \tag{12}$$

where λ is the wavelength of the large waves and includes only the sloped portions of the wave.

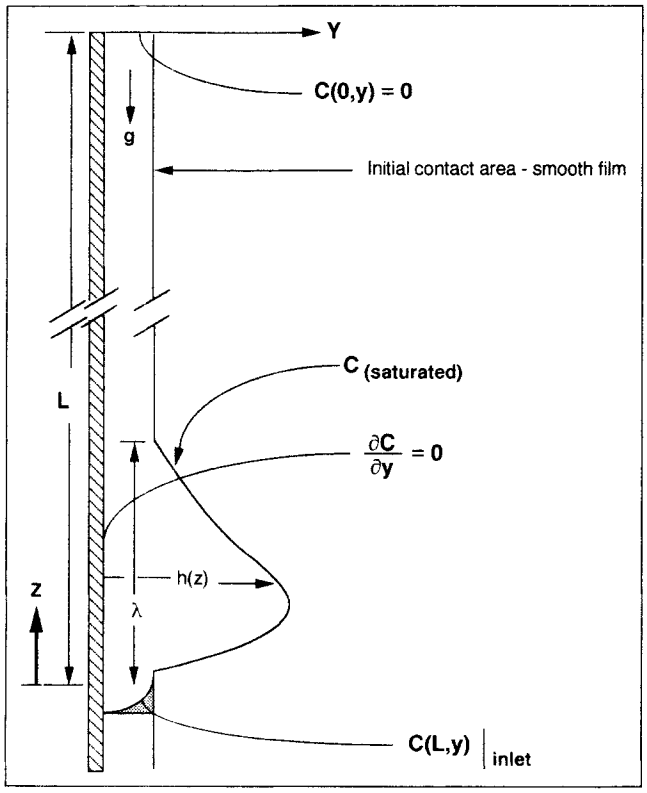

Figure 4. Absorption through large waves.

The solution of the transport problem was generated from a modified version of the finite-difference algorithm developed for the hydrodynamic problem (Wasden and Dukler, 1989b). In order to increase accuracy, a novel version of a quadratic upwind differencing technique, QUICK (Leonard, 1979), called NU-QUICK-ER was developed for approximating convective terms in both streamwise and normal directions. A mass source calculated using the concentration gradient at the surface was added to the mass conservation equation for those control volumes bordering the free interface, while no mass was allowed to leave the control volume through the wall. Details of the numerical method and surface treatment techniques appear elsewhere (Wasden, 1989).

The concentration field within each wave determined in this way was used to compute values of the local mass flux at the interface through Fick's law. Of particular interest is the mass flux integrated over the wavelength. The local flux given by the short contact theory can be integrated over the wavelength to yield

$$\int_{z=L-\lambda}^{L}\left[-D\left(\frac{\partial c}{\partial y}\right)_{y=h_N}\right]dz = \sqrt{\frac{gD\,h_N^2}{2\pi\nu}}\left[\sqrt{L} - \sqrt{(L-\lambda)}\right] \tag{13}$$

Grid refinement studies showed that the grid mesh necessary to fully resolve hydrodynamic details in the large waves provided sufficient detail for transport modeling. Approximately 2,000

mesh cells were used in each case. The iterative solution of the transport problem was continued until the sum of mass residuals throughout the wave was less than one part in 10^8 of the total mass transferred across the interface. Execution time for the code was between 200 and 300 CPU seconds on an NAS 9000 mainframe computer.

Mass tansfer from the wall

Mass transfer from the wall was computed by tracking the evolution of concentration profiles with time as the waves traversed the soluble surface. The total amount of mass accumulated by a wave was compared to that numerically computed for a smooth film having the same time of exposure to determine the enhancement due to the presence of the wave.

This simulation procedure required an algorithm designed specifically for unsteady simulations. The physical situation described by the model is shown in Figure 5. For this problem, the unsteady convective-diffusion equation is given by Eq. 1 with the coordinates as defined in Figure 5. Time begins when the wave front reaches the upper end of the active surface, where the film is assumed to be composed of pure solvent, Eq. 3a. Along the soluble surface, the concentration is equal to the value of a saturated solution, Eq. 5a, while no flux is allowed at the wall in regions outside the active region, requiring

$$\left(\frac{\partial c}{\partial y}\right)_{(x,0,t)} = 0, x < 0, x > L_A \tag{14}$$

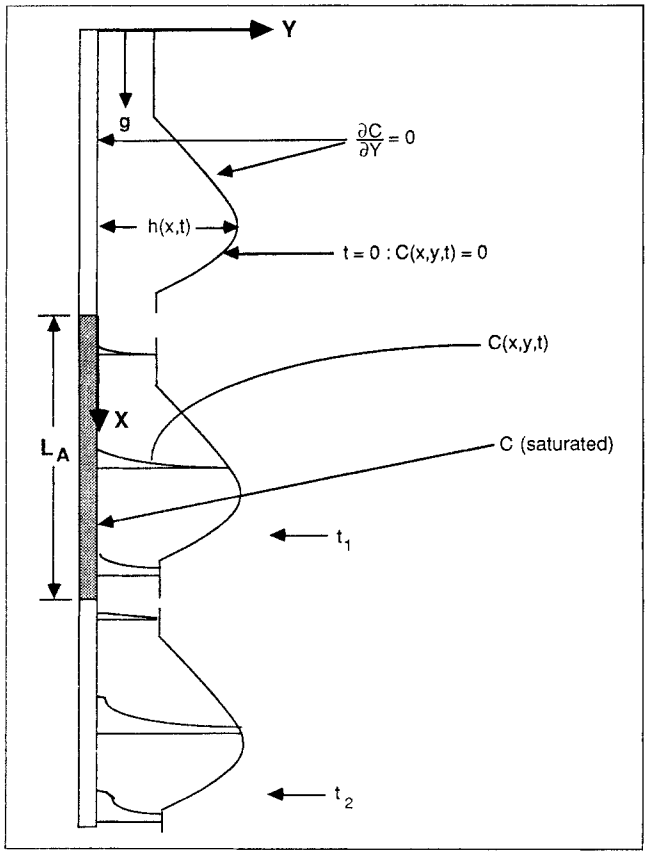

Figure 5. Mass transfer from solid boundary into a passing wave.

No mass is allowed to pass through the wavy interface, or

$$\left(\frac{\partial c}{\partial y}\right)_{[x,h(x,t),t]} = 0, -\infty < x < \infty, t > 0. \tag{15}$$

The problem formulation includes two parameters, the length of the active surface, L_A, and the Schmidt number. As in the case of mass transfer to the interface, the simulation used the same rectangular grid mesh as the hydrodynamic simulation; roughly 2,000 grid points were specified for each large wave. The small grid spacing used near the wall to resolve the wall shear stress in the hydrodynamic problem was suitable for the mass transfer problem where the concentration varied rapidly near the wall.

The unsteady term in the convection-diffusion equation was approximated with a first-order implicit finite-difference technique as recommended by Patankar (1980). The unsteady term adds a source term to the discretized equations that is easily assimilated into the control-volume-based method on which the algorithm was based. The implicit method is unconditionally stable for the present problem, insuring that the temporal behavior of the results are reasonable approximations to the true solution. To reduce errors in the solution, time step sizes of less than 1 ms were used.

The solution procedure began with the concentration field set to zero. As time advanced one step, the wave moved a distance determined by the velocity near the wall for the first grid cell. The first streamwise wall cell was specified as having a constant concentration boundary condition, therefore allowing a flux of solute, while all other wall cells were bounded by the solid wall, with a no-flux condition imposed. At this location and time, the concentration field was determined by solving the system of linear equations representing the finite-difference form of Eq. 1 using an alternating direction implicit (ADI) technique. This iterative technique was continued until the solution had converged to within one part in 10^8. The wave was then allowed to move downward another time step. The distance moved with each time step depended on the velocity associated with each grid near the wall; the algorithm adjusted the time step such that each step corresponded to moving the wave sufficiently that one more whole grid cell was subject to a flux condition. The grid mesh spacing in the streamwise direction was specified such that smaller grids were assigned to regions in which the velocity fields were changing rapidly. This grid spacing scheme insured that smaller time steps were taken in these regions, and that the mass transport was accurately approximated. Implicit in the simulation is the condition that each wave continues to evolve in the same way that was determined for a single location. This assumption is justified for an isolated wave changing very little with distance. In contrast, evolving and interacting waves are probably not well described by this criteria over a long distance. The present simulation will be limited to reasonably short active surface lengths in order to minimize this error.

Concentration fields were determined for each wave for fixed values of the active surface length and various Schmidt numbers. The algorithm required about 1 CPU second (on an NAS 9000 computer) for each time step, and for most cases, 200–300 CPU seconds were sufficient to complete each simulation.

Average Wave Structure of the Falling Film

An average wave structure was defined from time records of film thickness measurements taken at $Re = 880$ to determine

whether the statistically defined average wave, if distributed along the surface, would yield computed mass transfer rates comparable to experimental values. The film is modeled as periodic average waves separated by a rippled substrate.

Film thickness data from which the large wave profiles were taken were examined to determine the characteristics of an average large wave. Figure 6 illustrates the components of the proposed film structure, a series of triangular waves traveling over a flat substrate. Data consisting of 45 s of film thickness signals taken at two locations and sampled at 1kHz per channel were analyzed using traditional statistical techniques to arrive at the dimensions and velocity of the wave structure.

The wave velocity was determined by dividing the distance separating two film thickness probes (63 mm) by the time delay of the maximum of the cross-covariance of the signals. The time of the first zero of the film thickness autocorrelation provided an average wave frequency, f, from which the total length of the wave in the time domain was determined as

$$\frac{1}{f} = t_f + t_b + t_s \tag{16}$$

where t_f, t_b, and t_s are the lengths (in a time domain) of the front of the wave, the tail, and the separating substrate. Averaging over the ensemble of all measured waves separated by a substrate thinner than the mean thickness provided average values for t_f and t_b. The extent of the substrate, t_s, is then determined using Eq. 16.

The average substrate thickness, h_s, was chosen as the value below which 5% of the film thickness points fell. This value approximates the average of the minimum values of film thickness between large waves. With this value, the problem was closed using the volume conservation equation

$$h_N = h_s + \left(\frac{h_p - h_s}{2}\right)\frac{(t_b + t_f)}{(t_s + t_f + t_b)} \tag{17}$$

which can be solved for the peak thickness,

$$h_p = \left[\frac{2\,(h_N - h_s)\,(t_b + t_f + t_s}{(t_b + t_f)}\right] + h_s \tag{18}$$

The experimental data analyzed with this method had an average thickness, h_N, of 0.365 mm, an average substrate thickness, h_s, of 0.260 mm, and an average peak thickness, h_p, equal to 0.614 mm. The peak to substrate ratio is 2.36. An average frequency of 6.9 Hz was computed, along with average t_f of 33.3 ms and t_b of 51.0 ms. The substrate duration, t_s, was computed to be 60.7 ms. The wave velocity for the film was determined to be 1.15 m/s. Streamlines resulting from the hydrodynamic simulation of the average wave are shown in Figure 7.

Results

Gas absorption through the wavy interface

Simulations were carried out for seven large waves whose profiles were measured 3.1 m below the feed and which were representative of all isolated and interacting waves. For each wave, the Schmidt number was varied from 250 to 1,000, while the distance below the feed ranged from 1,000 to 6,000 Nusselt thicknesses. This parameter space encompasses nearly all industrially important gas–liquid diffusion systems and column heights. For each of the parameter pairs, a concentration field was determined. The local variation of mass flux could then be computed from the gradient of this concentration at the interface and the total flux through the interface determined from the integration of this local flux along the wave. Two waves will be discussed in detail: an isolated wave with peak/substrate thickness of approximately three and an interacting wave. Streamline maps for these waves are given in Figures 8 and 9.

Concentration fields computed for the isolated large wave are shown in Figure 10 for Schmidt numbers of 500 and 1,000 at a distance of 4,500 mean film thicknesses below the feed (1.63 m for a Reynolds number of 880). These conditions are comparable to those investigated experimentally by Emmert and Pigford (1954). The concentration profiles are presented as contour plots with intervals of 0.1 saturated concentration units dividing successive contour lines. Both concentration profiles show significant deviations from parallel isoconcentration lines predicted by the short contact time theory (SCTT). Normal (v) velocities within the wave peak carry solute from the surface into the wave. Near the front and rear of the wave, normal velocities resulting from the wave peak interacting with the substrate force the solute into the substrate. The effect of the Schmidt number is seen in the extent to which the concentration field penetrates the wave substrate; for a higher Schmidt number, this penetration occurs to a lesser extent.

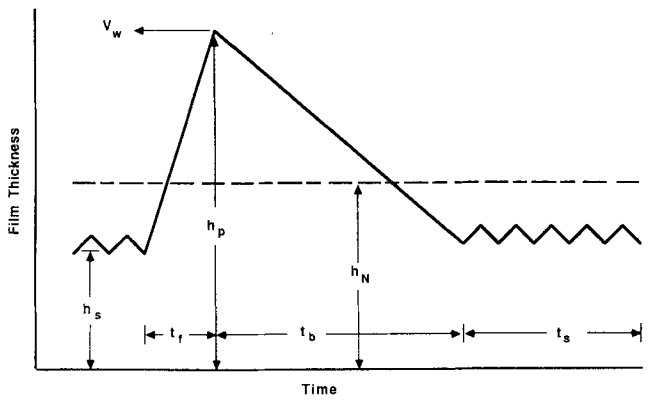

Figure 6. Average film structure dimensions.

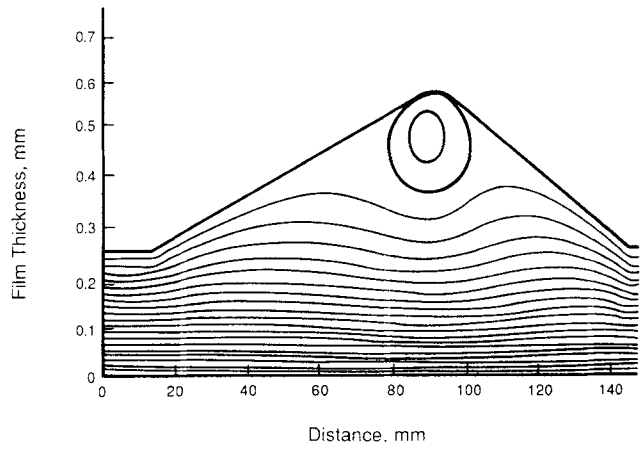

Figure 7. Streamline map for average large wave.

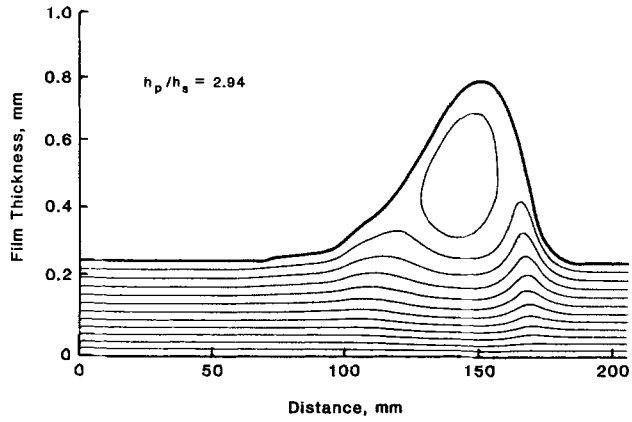

Figure 8. Streamline map for representative isolated wave.

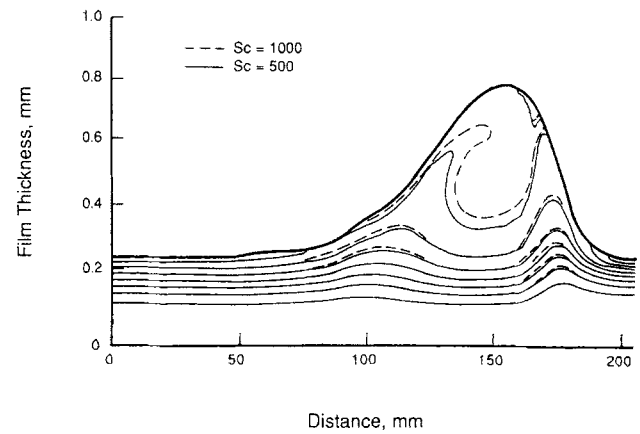

Figure 10. Concentration profiles in isolated wave 4,500 mean film thicknesses below feed for Schmidt nos. 500 and 1,000.

A profile of the local mass flux (for a saturated concentration of 1 kg/m^3) for the isolated wave is presented in Figure 11 for a Schmidt number of 500. The absence of normal velocities near the interface greatly affects the local flux near the front and rear stagnation points, where the local fluxes approach those expected for a purely diffusive situation. In contrast, near the front and behind the peak of the wave, convection increase the local flux by several times over the diffusive limit. Comparison of Figures 10 and 11 shows that the maxima in local flux values correspond to regions in which the wave peak interacts with the slowly moving substrate. This hydrodynamic process is also responsible for the dramatic increase in wall shear stress over that for parallel flow. Concentration and local flux profiles for the average wave were similar to those computed for the isolated wave. Previous models that suggest surface renewal as a result of large waves interacting with the substrate are now seen as clearly inconsistent with the computed concentration profiles.

Figure 12 shows the concentration profile in an interacting wave for a Schmidt number of 500 appearing 4,500 mean film thicknesses below the feed. The local flux profile for this interacting wave is shown in Figure 13. The profile appears to approximate the sum of the profiles obtained from isolated waves. The extra stagnation points create additional extrema in the profile, with the minimum occurring in the trough between the waves as a result of the stagnation region separating the two counterrotating recirculation zones. The presence of the stagnant zone separating the peaks dampens the effect of the interacting waves on mass transport. Compared to the SCTT prediction, enhancements are close to those associated with isolated waves.

The integral of the local flux along the wave was normalized by that expected for SCTT as given in Eq. 13. The predicted mass transfer to an isolated wave was then computed by weighting the flux through the wavy interface and the rippled substrate. Since the substrate was covered with capillary waves it was modeled using an enhancement of 30% as given by the model of Ruckenstein and Berbente (1968). The enhancement for the wave and its associated substrate was then computed from:

$$\frac{\text{Total flux}}{\text{SCTT prediction}} = \left(\frac{t_f + t_b}{t_f + t_b + t_s}\right)\frac{\text{Flux due to wave}}{\text{SCTT prediction}} + \left(\frac{t_s}{t_f + t_b + t_s}\right)(1.30) \quad (19)$$

Enhancement factors computed for the seven waves whose profiles were measured are presented in Figure 14 for several

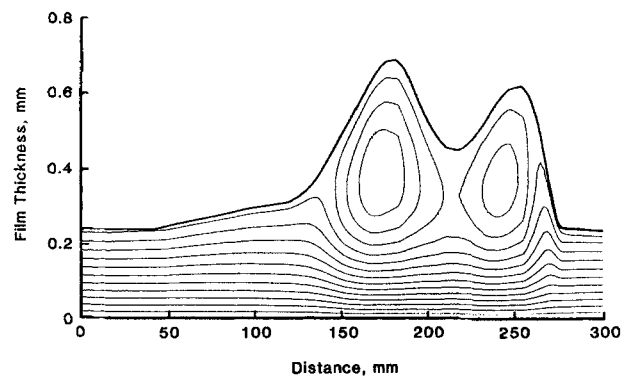

Figure 9. Streamline map for representative interacting wave.

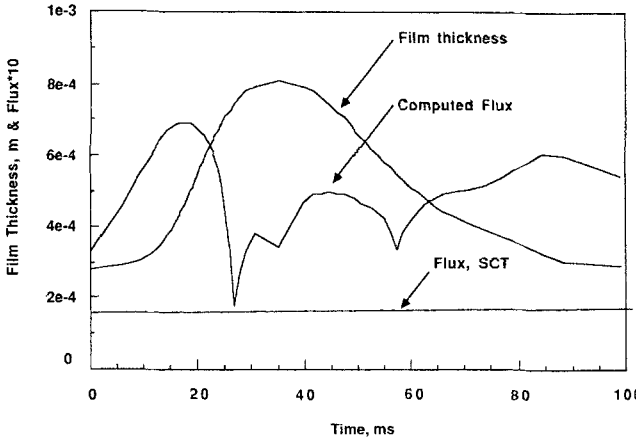

Figure 11. Local mass flux values for isolated wave for conditions of Figure 10 and *Sc* = 500.

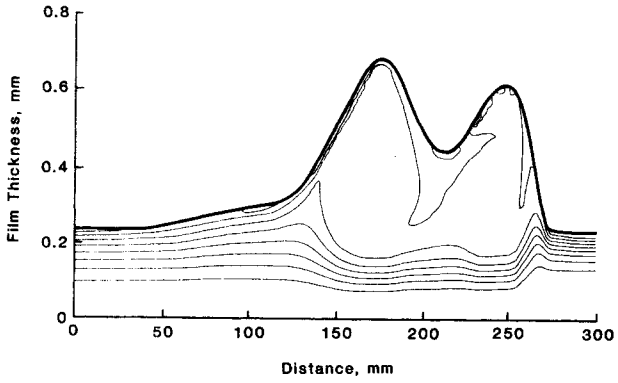

Figure 12. Concentration profiles in interacting wave 4,500 mean film thicknesses below feed for $Sc = 500$.

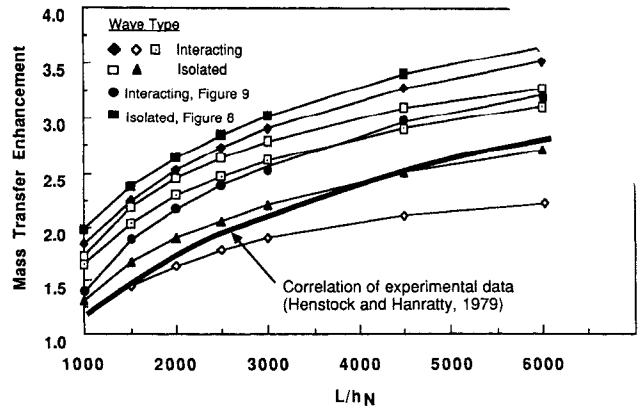

Figure 14. Computed and observed mass transfer enhancement for transfer through wavy interface at $Sc = 500$.

locations below the entry. It should be recognized that the wave profile and velocity vary along the length of the film (Zabaras and Dukler, 1988) while for these computations the profile measured at $L/h_N = 8{,}550$ (3.1 m) was used for the mass transfer computation at all locations. The numerical analysis predicts mass transfer rates 1.7–3.5 times greater than the short contact time predictions. A comparison with experimental data as correlated by Henstock and Hanratty (1979) is included in this figure. The experiments represent mass transfer rates averaged from L/h_N of zero to the indicated value while the computation describes the local rate as the wave passes a particular L/h_N. Similar qualitative trends in enhancement are clearly seen in both computed and measured values.

Figure 15 compares the enhancement computed for the average wave uniformly distributed across the length of the interface with the experimental enhancement given by the Henstock and Hanratty (1979) correlation. The agreement in magnitude and trend is now semiquantitative. Furthermore, the discrepancies can readily be understood. For short columns the waves are smaller and the rate of mass transfer would be less than that computed for the average film structure in the figure. At large values of L/h_N the existence of waves above this location changes the inlet condition used in the computations to one of a more uniform concentration as a result of the successive mixing induced by the upstream waves. This would lead to larger concentration gradients at the surface and consequently a higher mass transfer rate than predicted by the simulation. Inclusion of these effects would produce even closer agreement between the model and experiment. Once the ability to predict the average profile as a function of position along the film is developed these factors can readily be incorporated into the computation.

Mass transfer from the wall

Simulations of the mass transfer in the two waves discussed in the previous section will be presented. Concentration fields, average concentration values [across the film, from $y = 0$ to $y = h(x, t)$], and total mass accumulation were determined for fixed values of the active surface length and various Schmidt numbers. Mass transfer enhancement due to large waves was determined by computing the total mass within the large wave after it had passed over the active surface and comparing it to the amount of mass accumulated by a flat film of thickness h_N which had been in contact with the active surface for the same amount of time. The active surface length for the present results was 800 average film thicknesses, or roughly 0.29 m for a Reynolds number of 880. This value represents about one

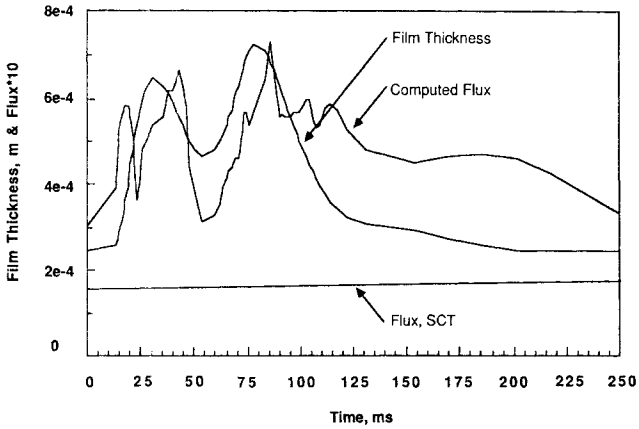

Figure 13. Local mass flux values for interacting wave for conditions of Figure 12.

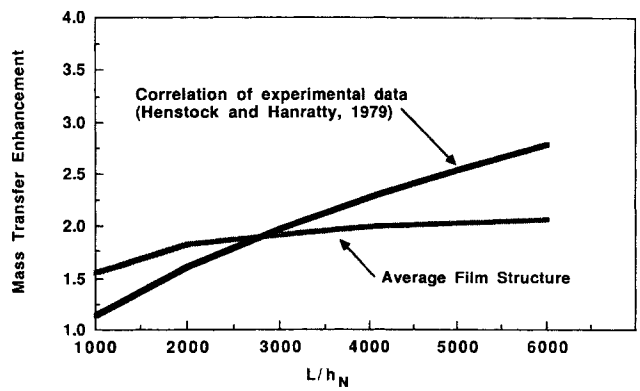

Figure 15. Mass transfer enhancement computed for average film structure compared to observed values for $Sc = 500$.

wavelength. Results for Schmidt numbers of 200 and 1,200 are presented. Fluid physical properties were taken as identical to those used for the hydrodynamic simulation, leading to Peclet numbers ranging from 1.76×10^5 to 1.056×10^6.

Average concentration profiles (normalized by the saturated wall concentration) for the isolated large wave are presented in Figure 16. The increase in average concentration ahead of the peak is due to the strong normal velocities at the wall in this region, which result from the rapid change in wall shear stress. The average concentration profiles appear to be affected most by the strong hydrodynamic interactions between the wave peak and body with the surrounding flat film. Other hydrodynamic processes caused by the wavy interface apparently do not penetrate to a level sufficient to alter the transport processes at the wall.

Further evidence of the strong normal velocities near the wall is found in the profiles of near wall concentrations, Figure 16b. The near wall concentrations are those that are found in the first cell inside the boundary and are proportional to the concentration gradient at the wall. These values are significantly lower directly under the steepest part of the wave front, which corresponds to the region in which the shear stress is a maximum. Average and near wall concentrations are closest in magnitude near the front and under the peak of the wave. In contrast, the surrounding regions of substrate are characterized by near wall and average concentrations that differ by as much as a factor of ten.

Increasing the Schmidt number reduces mass diffusivity, increasing the resistance to mass transport into the waves. However, the presence of significant normal velocities near the wall reduces this effect. For large Peclet numbers, increasing the Schmidt number sixfold (from 200 to 1,200) would be expected to decrease the average concentration by the same factor if no normal velocities were present. However, Figure 16a shows that the average concentration is reduced by no more than three when the hydrodynamic effects are included. In a flat film, the near wall concentrations would be expected to scale inversely with Schmidt number, as the flux is directly proportional to the diffusivity. Figure 16b shows that the near wall concentration decreases by no more than one-half when the Schmidt number is increased sixfold, further illustrating the extent to which normal velocities alter the mass transfer resistance.

Flow within the interacting wave produces the concentration profiles shown in Figure 17. The presence of two interacting but separate closed recirculation regions within the peaks significantly increases mass transfer through the wavy surface and apparently has the same effect on transport from the wall. Pronounced changes in the average concentration accompany increasing mass diffusivity in the interacting wave. While the near wall concentration variation is magnified by low diffusivity, the variation in average values suggests that once the mass is transported into the peak regions, diffusion becomes important, as the average concentration profile associated with a lower diffusivity is smoother than expected.

Mass transfer enhancements for three interacting waves, the isolated wave, and the average film are presented in Figure 18. Experimentally determined enhancements from Stirba and

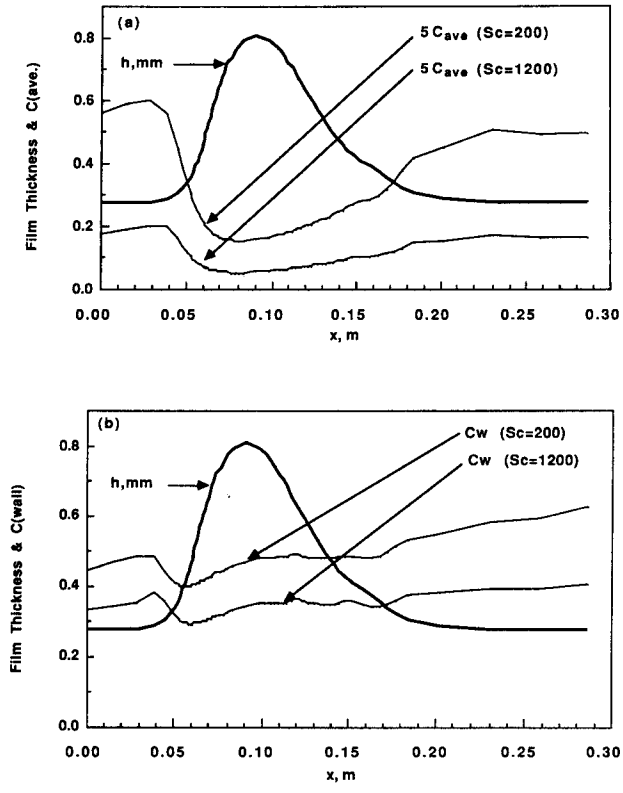

Figure 16. Variation of concentration with film thickness and Schmidt number for isolated wave.

(a) Average concentration
(b) Rear wall concentration.

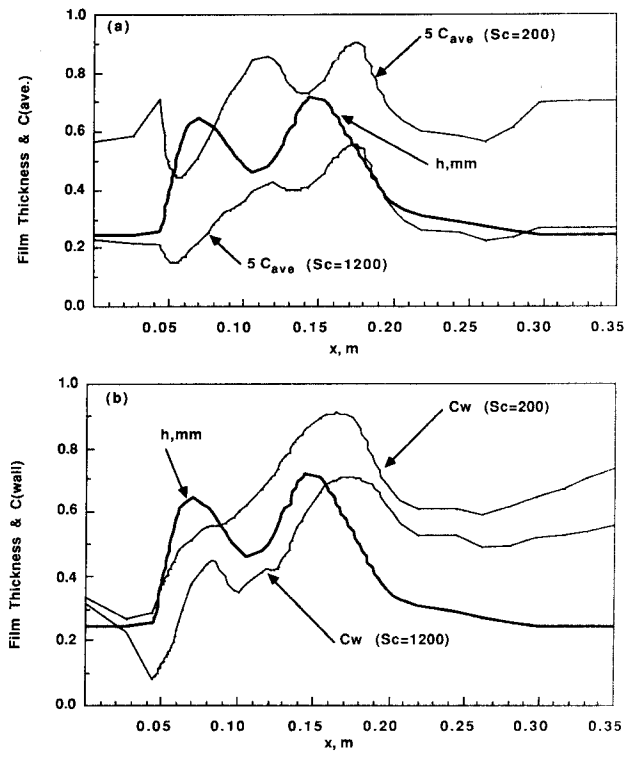

Figure 17. Variation of concentration with film thickness and Schmidt number for interacting wave.

(a) Average concentration
(b) Near wall concentration.

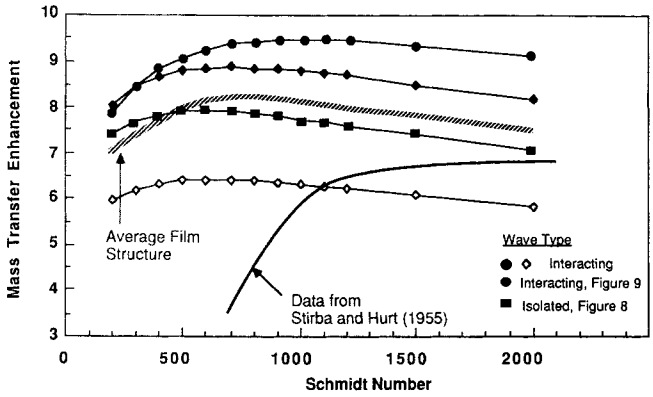

Figure 18. Computed and observed mass transfer enhancement for transfer from wall for *Re* = 880.

Hurt (1955) at Reynolds numbers between 850 and 900 are included for comparison. Values for the average film fall between the large waves and agree reasonablly well with the data at higher Schmidt numbers. At lower Schmidt numbers, the simulations appear to overpredict the enhancement. The discrepancy results from two experimental limitations. Stirba and Hurt report difficulties in fully wetting the surface of the benzoic acid with water (Schmidt number 609), which would decrease the accumulation by the wavy film. For alcohol–organic acid systems (Schmidt numbers > 800) no wettability problems were encountered and the comparison is correspondingly more favorable.

In the limit of very small Schmidt numbers, the enhancement due to the complex hydrodynamics vanishes, but for Schmidt numbers as low as 200 this enhancement may still be as large as 500%. As the Schmidt number increases above roughly 1,200 the enhancement associated with large waves begins to decrease due to the inability of the fluid to diffuse into the regions of the flow in which normal (v) velocities exist. It is expected that for Schmidt numbers of industrial interest, normally less than 5,000, the enhancement due to large wave hydrodynamics will be at least 500%.

Conclusions

The interface of a falling liquid film is covered with a random array of small and large waves interacting in a complicated manner, including many with peak thicknesses several times the mean. Neglecting the influence of the large waves causes most models to seriously underpredict experimentally observed transfer rates. Numerical simulations of the hydrodynamics within large waves presented previously (Wasden and Dukler 1989a, b) exposed mechanisms through which transport would be augmented. Hydrodynamic data obtained from this procedure were used in the simulation of passive transport in these large waves. The importance of the complex hydrodynamics within the waves has been demonstrated by the semiquantitative agreement between computed and measured transfer rates at both interfaces. Future modeling of transport processes in wavy films must include provisions for predicting the significant normal velocities at each interface and relating them to the interfacial structure.

The random interface has been approximated by an interface composed of periodically occurring, statistically average waves interspersed among smaller ripples. Mass transfer rates computed for such an array are 1.5 to 2.5 times greater than that predicted for gas absorption into nonwavy films and four to seven times greater than the flat film prediction for a dissolving wall. These enhancements are in reasonable agreement with experimental observations.

Acknowledgment

Financial support of this research by the Office of Naval Research is gratefully acknowledged. F. K. Wasden was supported by a National Science Foundation Graduate Fellowship.

Notation

c = local contaminant concentration, kg/m^3
D = gas–liquid or liquid–liquid diffusion coefficient, m^2/s
E = mass transfer rate enhancement, Eq. 6
f = average wave frequency, Hz
g = acceleration of gravity, m/s^2
h = local film thickness, mm
h_s = substrate thickness of average wave, mm
h_p = peak thickness of average wave, mm
h_N = time average, or Nusselt film thickness, mm
k_L = liquid-side mass transfer coefficient, m/s
L = length over which gas contacts a falling film, m
L_A = length of contaminated portion of wall, m
n = coordinate normal to wavy interface, m
N_{SCTT} = mass transfer rate predicted by short contact time theory, kg/m · s
Pe = Peclet number, $Re \cdot Sc$
Q = liquid film flow rate per unit perimeter, $U_N h_N$, m^2/s
Re = film Reynolds number, $4Q/\nu$
Sc = Schmidt number, ν/D
t_b = duration of average wave back, ms
t_f = duration of average wave front, ms
t_s = duration of substrate separating average waves, ms
u = local streamwise velocity, m/s
U_N = time average, or Nusselt film velocity, m/s
v = local velocity normal to boundary, m/s
V_w = wave velocity, m/s
x = axial coordinate in lab frame, m
y = coordinate normal to boundary, m
z = axial coordinate fixed on wave, m

Greek letters

ρ = liquid density, kg/m^3
ν = liquid kinematic viscosity, m^2/s
μ = liquid absolute viscosity, kg/m s
τ_w = wall shear stress, N/m^2
λ = length of sloped sections of large wave, m

Literature Cited

Acrivos, A., "Solution of the Laminar Boundary Layer Energy Equation at High Prandtl Numbers," *Phys. Fluids*, **3**, 657 (1960).
Bach, P., and J. Villadsen, "Simulation of the Vertical Flow of a Thin, Wavy Film Using a Finite-element Method," *Int. J. Heat Mass Transfer*, **27**, 815 (1984).
Back, D. D., and M. J. McCready, "Theoretical Study of Interfacial Transport in Gas–Liquid Flows," *AIChE J.*, **34**, 1789 (1988).
Banerjee, S., E. Rhodes, and D. S. Scott, "Mass Transfer to Falling Wavy Liquid Films at Low Reynolds Numbers," *Chem. Eng. Sci.*, **22**, 43 (1967).
Barrdahl, R. A. G., "Mass Transfer in Falling Films: Influence of Finite-amplitude Waves," *AIChE J.*, **34**, 493 (1988).
Benjamin, T. B., "Wave Formation in Laminar Flow Down an Inclined Plane," *J. Fluid Mech.*, **2**, 554 (1957).
Brumfield, L. K., R. N. Houze, and T. G. Theofanous, "Turbulent Mass Transfer at Free, Gas–Liquid Interfaces, with Applications to Film Flows," *Int. J. Heat Mass Transfer*, **18**, 1077 (1975).
Davies, J. T., *Turbulence Phenomena*, Academic Press, London (1972).

Dukler, A. E., "The Role of Waves in Two-phase Flow: Some New Understanding," *Chem. Eng. Educ.*, 1976 Award Lecture, 108 (1977).
Emmert, R. E., and R. L. Pigford, "A Study of Gas Absorption in Falling Liquid Films," *Chem. Eng. Prog.*, **50,** 87 (1954).
Goren, S. L., and R. V. S. Mani, "Mass Transfer through Horizontal Liquid Films in Wavy Motion," *AIChE J.*, **14,** 57 (1968).
Gosman, A. D., and F. J. K. Ideriah, *Teach-T: A General Computer Program for Two-dimensional, Turbulent, Recirculating Flows,* Dept. Mech. Eng., Imperial College, London (1976).
Hanratty, T. J., and J. A. Campbell. "Measurement of Wall Shear Stress," *Fluid Mechanics Measurement,* R. J. Goldstein, ed., Hemisphere (1983).
Henstock, W. H., and T. J. Hanratty, "Gas Absorption by a Liquid Layer Flowing on the Wall of a Pipe," *AIChE J.*, **25,** 122 (1979).
Howard, D. W., and E. N. Lightfoot, "Mass Transfer to Falling Films. 1: Application of the Surface-stretch Model to Uniform Wave Motion," *AIChE J.*, **14,** 458 (1968).
Javdani, K., "Mass Transfer in Wavy Liquid Films," *Chem. Eng. Sci.*, **29,** 61 (1974).
Kafesjian, R., C. A. Plank, and E. R. Gerhard, "Liquid Flow and Gas-phase Mass Transfer in Wetted-wall Towers," *AIChE J.*, **7,** 463 (1961).
Kapitza, P. L., and S. P. Kapitza, "Wave Flow in Thin Layers of a Viscous Fluid," *Zh. Exper. i Teor Fiz.*, **19,** 105 (1949), also in *Collected Papers of P. L. Kapitza,* II, Macmillan, New York (1964).
Leonard B. P., "A Stable and Accurate Convective Modeling Procedure Based on Quadratic Upstream Interpolation," *Comp. Meth. Appl. Mech. Eng.*, **12,** 59 (1979).
Levich, V. G., *Physicochemical Hydrodynamics,* Prentice-Hall, New York, (1962).
McCready, M. J., and T. J. Hanratty, "Effect of Air Shear on Gas Absorption by a Liquid Film," *AIChE J.*, **31,** 2066 (1985).
McCready, M. J., E. Vassiliadou, and T. J. Hanratty, "Computer-simulation of Turbulent Mass Transfer at a Mobile Interface," *AIChE J.*, **32,** 1108 (1986).
Nakaya, C., "Waves on a Viscous Fluid Film Down a Vertical Wall," *Phys. Fluids,* **A1,** 1143 (1989).
Oliver, D. R., and T. E. Atherinos, "Mass Transfer to Liquid Films on an Inclined Plane," *Chem. Eng. Sci.*, **23,** 525 (1968).
Pantakar, S. V., *Numerical Heat Transfer and Fluid Flow,* Hemisphere, Washington, DC (1980).
Pigford, R. L., Ph.D. Thesis, Univ. Illinois (1941).
Portalski, S., and A. J. Clegg, "Interfacial Area Increase in Rippled Film Flow in Wetted Wall Columns," *Chem. Eng. Sci.*, **26,** 773 (1971).
Ruckenstein, E., and C. P. Berbente, "Mass Transfer in Wave Flow," *Chem. Eng. Sci.*, **20,** 795 (1965).
———, "Mass Transfer to Falling Liquid Films at Low Reynolds Numbers," *Int. J. Heat Mass Transfer,* **11,** 743 (1968).
Seban, R. A., and A. Faghri, "Wave Effects on the Transport to Falling Laminar Liquid Films," *J. Heat Transfer,* **100,** 143 (1978).
Spence, D. A., and G. L. Brown, "Heat Transfer to a Quadratic Shear Profile," *J. Fluid Mech.*, **33,** 753 (1968).
Stirba, C., and D. M. Hurt, 'Turbulence in Falling Liquid Films," *AIChE J.*, **1,** 178 (1955).
Suzuki, K., Y. Hagiwara, and T. Sato, "Heat Transfer and Flow Characteristics of Two-phase Two-component Annular Flow," *Int. J. Heat Mass Transfer,* **26,** 597 (1983).
Telles, A. S., and A. E. Dukler, "Statistical Characteristics of Thin, Vertical, Wavy, Liquid Films," *Ind. Eng. Chem. Fundam.*, **9,** 412 (1970).
Wasden, F. K., "Studies of Mass and Momentum Transfer in Free Falling Wavy Films," *Ph.D. Diss.*, Univ. Houston (1989).
Wasden, F. K., and A. E. Dukler, "Insights into the Hydrodynamics of Free Falling Wavy Films," *AIChE J.*, **35,** 187 (1989a).
———, "Numerical Investigation of Large Wave Interactions on Free Falling Films," *Int. J. Multiph. Flow,* **15,** 357 (1989b).
Zabaras, G. J., and A. E. Dukler, "Countercurrent Gas–Liquid Annular Flow, Including the Flooding State," *AIChE J.*, **34,** 389 (1988).

Manuscript received Nov. 30, 1989, and revision received July 6, 1990.